
TRANSFUSION: CONTRASTIVE LEARNING WITH TRANSFORMERS

A PREPRINT

Huanran Li

Department of Electrical Engineering
Wisconsin Institute of Discovery
University of Wisconsin-Madison
Madison, WI 53705
hli488@wisc.edu

Daniel Pimentel-Alarcón

Department of Biostatistics and Medical Informatics
Wisconsin Institute of Discovery
University of Wisconsin-Madison
Madison, WI 53705
pimentelalar@wisc.edu

March 28, 2024

ABSTRACT

This paper proposes a novel framework, *TransFusion*, designed to make the process of contrastive learning more analytical and explainable. *TransFusion* consists of attention blocks whose softmax being replaced by ReLU, and its final block's weighted-sum operation is truncated to leave the adjacency matrix as the output. The model is trained by minimizing the *Jensen-Shannon Divergence* between its output and the target affinity matrix, which indicates whether each pair of samples belongs to the same or different classes. The main contribution of *TransFusion* lies in defining a theoretical limit for answering two fundamental questions in the field: the maximum level of data augmentation and the minimum batch size required for effective contrastive learning. Furthermore, experimental results indicate that *TransFusion* successfully extracts features that isolate clusters from complex real-world data, leading to improved classification accuracy in downstream tasks.

1 Introduction

Contrastive Learning (CL) has recently garnered significant attention due to its effectiveness in training feature extraction models without the need for labeled data. Along this trajectory, several renowned models have been introduced, including SimCLR[1], Contrastive Multiview Coding (CMC) [2], VICReg[3], BarLowTwins[4], and [5, 6]. These approaches share a common framework: during training, the objective is to minimize the distance between augmented versions of images from the same source while simultaneously maximizing the distance between images from different sources. Following the training phase, the model is commonly combined with a feed-forward neural (FFN) decoder to fine-tune its performance using labeled data. Empirical evidence demonstrates that these models can achieve performance levels comparable to fully-supervised models, even when trained with a relatively limited amount of labels (approximately 10%) on moderate to large datasets [7].

Recent studies in the field have revealed that contrastive learning is influenced by several factors. These include the methods used to augment data [8, 9, 10, 11, 12], the tuning of hyperparameters [13], the choice of optimizers [13], and the types of loss functions used [14, 15, 16, 17]. From these studies, there's a general consensus on a few best practices for enhancing the learning process in contrastive learning. Two of the most notable practices are using large batch sizes during training, as suggested by [1], and carefully tuning the data augmentation process, as recommended by [11]. However, it's important to note that these findings, despite being empirically observed and widely accepted, lack a solid theoretical foundation in the research community. This leaves some unanswered questions in training contrastive learning models, particularly regarding the minimum batch size and the optimal scale of data augmentation necessary for successful learning outcomes.

To address these key questions, we introduce a novel framework, *TransFusion*, designed to make the process of embedding learning more explainable. The key novelty behind *TransFusion* lies in defining a theoretical limit for data noise and batch size that leads to provable successful contrastive learning. This is a significant breakthrough as it

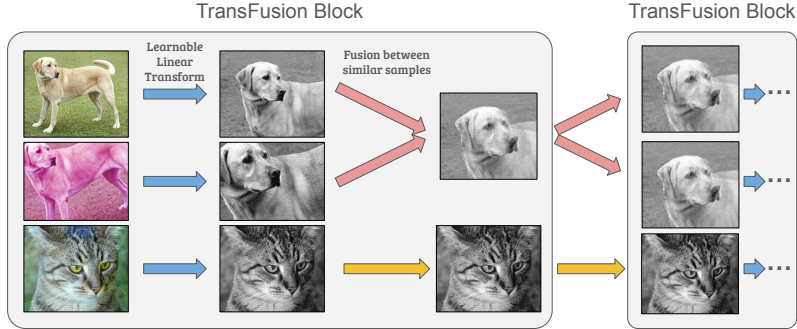


Figure 1: The fusion process within each *TransFusion* block. The model first learns an optimal linear transformation, which extracts distinctive information from the data. Following this, it computes the pairwise cosine similarities between all samples, and images that are found to be similar are then merged. This combined output becomes the input for the subsequent layer in the model.

answers two fundamental questions in the field: it establishes the optimal level of data augmentation needed, and the minimum batch size required for effective contrastive learning. This latter point is particularly relevant since there is a common belief in the contrastive learning community that larger batch size yield better results. This achievement is made possible by the unique and insightful architecture our *TransFusion* model, which enables a layer-wise fusion of embeddings, facilitating a more flexible learning process that our theory can characterize. Compared to other CL models, whose theoretical aspects in the context of classification tasks remain largely unknown, our theoretical results show that each layer excels at effectively fusing data points within the same cluster, while simultaneously ensuring careful management of noise levels.

TransFusion is structured as a sequence of attention blocks, within which the softmax function is substituted by an element-wise ReLU function. These blocks compute the pairwise cosine similarity scores between the inputs. Then, for samples that are found to be similar, they are combined using weighted-sum operations (example refers to Figure 1). In its final block, rather than completing the usual weighted-sum operation, the process is truncated, leaving the adjacency matrix as the output. The model is then fed a target affinity matrix, which indicates whether each pair of images belongs to the same or different classes. The training of the model revolves around minimizing the *Jensen-Shannon Divergence* between its output and this target affinity matrix. The aim is for the model to generate embeddings where samples of the same class are closer together in the embedding space. Both theoretical analysis and experimental results support the effectiveness of this approach. They show that each layer in the model progressively refines the input, creating embeddings that are not only denser but also distinct across different classes.

TransFusion stands out for several key advantages, most notably its explainability. To support this, we carried out a detailed theoretical analysis. The results clearly show that each layer within *TransFusion* plays an active role in the fusion process, as long as the noise level is kept within a certain limit. This finding is particularly useful in determining the maximum level of augmentation needed for effective fusion, especially when using images as inputs. Additionally, it sheds light on how the structure of classes, namely the distances within and between clusters, affects the fusion’s effectiveness. Another significant aspect of *TransFusion* is its flexible approach to managing the loss function. Traditional contrastive loss functions operate under the assumption that all samples within the same class should have identical similarities, ignoring the natural variations in proximity or distance among samples in the same class. *TransFusion*, however, offers a more nuanced approach. Its fusion process can be seen as a relaxation of the loss function, allowing for the formation of denser clusters where samples from the same class exhibit similar, but not identical, similarities. Moreover, *TransFusion* is designed to be highly adaptable and can be easily integrated as a plugin with any existing network.

Paper Organization. We provide a formal introduction to *TransFusion* and its key insights in Section 2. Subsequently, we conduct a comprehensive theoretical analysis of *TransFusion* in Section 3. Moving forward, we delve into the landscape of relevant research pertaining to neural network embedding learning in Section 4. To validate the efficacy of our approach, we present the experimental results in Section 5.

2 TransFusion

In this section, we present our primary contribution: *TransFusion*. Initially, we provide a mathematical definition of the model and elucidate the underlying principles of the fusion process. Subsequently, we describe the custom-

tailored loss function employed in *TransFusion*, which is optimized to enhance the effects of contrastive learning. The fundamental objective of *TransFusion*, akin to other contrastive learning models, is to generate embeddings that proficiently differentiate between various classes. This entails that samples from the same class should exhibit closer proximity in the embedding space in comparison to those from disparate classes.

2.1 Model

To achieve this goal, *TransFusion* takes a batch of input samples and generates a non-negative affinity matrix, which reflects the similarities between pairs of samples. Higher values in the affinity matrix at the i, j 'th entry indicate stronger similarities between sample i and sample j . The model is then trained by minimizing the Jensen-Shannon Divergence (JSD; more on this choice below) between the output affinity matrix and a target affinity matrix, which denotes as $\mathbf{Y} \in \{0, 1\}^{n \times n}$:

$$[\mathbf{Y}]_{ij} = \begin{cases} 1 & i, j \text{ in the same class and } i \neq j, \\ 0 & \text{otherwise.} \end{cases} \quad (1)$$

TransFusion adeptly manages two distinct scenarios: (i) the unsupervised case, wherein affinity is determined through data augmentation, and (ii) the supervised case, where affinity is established based on class labels.

Similar to Transformer, *TransFusion* also consists of identical TransFusion blocks. Denote the input matrix as $\mathbf{X} \in \mathbb{R}^{n \times m}$, where m represents the ambient dimension, and n represents the batch size. Furthermore, if we denote \mathbf{X}^ℓ as the input of the ℓ 'th *TransFusion* block, then ℓ 'th block can be defined as:

$$\mathbf{A}^\ell := (\mathbf{X}^\ell \mathbf{W}_Q^\ell)(\mathbf{X}^\ell \mathbf{W}_K^\ell)^\top, \quad (2)$$

$$\mathbf{X}^{\ell+1} := \text{ReLu}(\mathbf{A}^\ell)(\mathbf{X}^\ell \mathbf{W}_V^\ell) + \mathbf{X}^\ell, \quad (3)$$

where \mathbf{W}_Q^ℓ , \mathbf{W}_K^ℓ , and $\mathbf{W}_V^\ell \in \mathbb{R}^{m \times m}$ represent the learn-able parameters. For training stability and subsequent analysis, \mathbf{X}^ℓ are normalized before every block ℓ so that each entry has unit length. The output of the *TransFusion* is the last block's affinity matrix \mathbf{A}^d , where d is the number of blocks in the *TransFusion*.

To gain deeper insight into the *TransFusion* model's functioning, let us delve into the three key components: queries $\mathbf{X}\mathbf{W}_Q$, keys $\mathbf{X}\mathbf{W}_K$, and values $\mathbf{X}\mathbf{W}_V$. The output of each block is obtained by calculating cosine-similarity queries and keys, and then aggregating a similarity-weighted sum of the values. Under this mechanism, if the model learns an effective linear transformation of queries and keys, the similarity between samples from the same class can be high, whereas the similarity from the different class can be low. Using this as the weight in the next weighted-sum calculation, samples from the same class shall be able to fuse closer to each other (as demonstrated in Figure 1). To further leverage this fusion effect, we change the softmax function in the original attention block to elemental-wise ReLU, which gives us important advantages:

- **Increased clustering flexibility:** By adopting elementalwise ReLU, multiple elements with high similarity scores can fuse into the same cluster. This approach facilitates the integration of a broader range of elements into clusters.
- **Enhanced model non-linearity:** It is important to note that the model does not necessarily require a feed-forward layer immediately after each attention block. However, by incorporating an activation function at this stage, we introduce non-linearity into the model, thereby fortifying its resilience and adaptability.

2.2 Loss Function

Our training objective is to minimize the Jensen-Shannon divergence between the last block's affinity matrix \mathbf{A}^d and the target affinity matrix \mathbf{Y} :

$$\begin{aligned} \mathcal{L}_{\text{TF}}(\mathbf{A}^d, \mathbf{Y}) := & \sum_{i,j} [\mathbf{Y}]_{i,j} \frac{[\mathbf{Y}]_{i,j}}{g([\mathbf{A}^d]_{i,j})/2 + [\mathbf{Y}]_{i,j}/2} \\ & + \sum_{i,j} [\mathbf{A}^d]_{i,j} \frac{[\mathbf{A}^d]_{i,j}}{g([\mathbf{A}^d]_{i,j})/2 + [\mathbf{Y}]_{i,j}/2} \end{aligned} \quad (4)$$

where $g(\cdot)$ is a normalizing function that converts real numbers into probabilities, specified as:

$$g(\mathbf{A}^d) := \text{Row-Normalize}((\mathbf{A}^d)^2) \quad (5)$$

Remarkably, if we use *Kullback-Leibler Divergence* [18] instead, and set $g(\cdot)$ to be the row-wise *Softmax*, our loss with a one-layer *TransFusion* model behaves identically to *InfoNCE* and *SupCon*. The detailed proof is available in Appendix A. The reasoning behind our choice of loss is based on the following considerations:

- *KL-Divergence*'s inherent asymmetry becomes particularly problematic the context where a majority of entries in \mathbf{Y} are filled with zeros. To see this, take any pair of samples i and j belonging to different classes, the loss term $\left([\mathbf{Y}]_{i,j} \log \frac{[\mathbf{Y}]_{i,j}}{[g(\mathbf{A})]_{i,j}}\right)$ prevents the model from penalizing the positive value of the affinity term $[g(\mathbf{A})]_{i,j}$ as the target affinity is zero, i.e. $[\mathbf{Y}]_{i,j} = 0$. Although the normalization within g might indirectly influence $[g(\mathbf{A})]_{i,j}$ to be small, this effect is relatively minor compared to the influence other terms. In simpler terms, this loss function strongly encourages embeddings from the same class to be close to each other while largely disregarding the distances between embeddings from different classes. *Jensen-Shannon Divergence*, on the other hand, is a symmetric loss that avoids singularity with target affinities being zero.
- *Softmax* converts negative values to low probability. However, in our unique context, such negativity does not necessarily signify insignificance. To illustrate, consider the case two embedding vectors $\mathbf{z}_i, \mathbf{z}_j$ lies in the same linear subspace, we can ensure that the magnitude of the affinity is large, possibly equal to $\|\mathbf{z}_i\|_2 \|\mathbf{z}_j\|_2$. However, we cannot tell whether two vectors face the same direction or exact opposite directions. This latter scenario results in a negative projection value. If negative values are converted to low probabilities, as done by *Softmax*, it can limit the model's ability to effectively discern and utilize the underlying substructures within the embedding space. To address this, we square the entries in the affinity matrix. By doing so, we treat both negative and positive affinities equally, allowing for a more flexible and effective use of the embedding space.

Through our ablation studies (Appendix B), we have uncovered an enhancement in stability of our custom loss function (4) and (5) in comparison to alternative choices, including *InfoNCE*. This improvement is evident in both performance and resilience to changes in the learning rate.

3 Theoretical Guarantees

In the first half of this section we will focus on the noiseless setting to show that if the input data matrix \mathbf{X} exhibits a structure of subspace clusters, then a single-layer *TransFusion* model can accurately produce an affinity matrix that distinguishes samples within the same subspace. We consider the data matrix \mathbf{X} to consist of multiple low-dimensional subspaces, represented as $\{\mathcal{U}_1, \dots, \mathcal{U}_{\mathcal{K}}\}$, where each row of \mathbf{X} is part of one of these subspaces, with the rank of each subspace not exceeding r . We assume that no single subspace is linearly dependent on a combination of all other subspaces, i.e. $(\mathcal{K} - 1)r < m$, where m denotes ambient dimension and maximum rank of \mathbf{X} .

In the second part of this section, we generalize our results to show that in the presence of noise, each layer of *TransFusion* effectively merges samples from the same class. Our theoretical findings indicate that the outcomes of contrastive learning are primarily influenced by the noise level, the spatial distance between clusters, and the batch size.

3.1 Noise-Free Fusion

For each low-rank subspace \mathcal{U}_k , there always exists a unit vector \mathbf{u}_k^\perp that is perpendicular to \mathcal{U}_k , such that for any vector \mathbf{x}_i not belonging to \mathcal{U}_k , the cosine similarity between \mathbf{x}_i and \mathbf{u}_k^\perp is non-zero. Furthermore, we introduce *Cluster Integrity* as a measurement of the lower bound of the maximum cosine-similarity.

Definition 1. Given a collection of input samples \mathbf{X} , where each sample \mathbf{x}_i belongs to one of the subspaces among $\{\mathcal{U}_1, \dots, \mathcal{U}_{\mathcal{K}}\}$, the **Cluster Integrity** ρ is defined as the lower bound of $\{\rho_1, \dots, \rho_{\mathcal{K}}\}$, where

$$\rho_k := \max_{\mathbf{u} \perp \mathcal{U}_k} \min_{\mathbf{x}_i \notin \mathcal{U}_k} |\mathbf{x}_i^\top \mathbf{u}| \quad (6)$$

In words, *Cluster Integrity*, ranging from 0 to 1, measures the degree of separation between subspace clusters. If two clusters \mathcal{U}_a and \mathcal{U}_b are well-separated, then a vector \mathbf{u}_a^\perp , orthogonal to \mathcal{U}_a , can be found for large cosine-similarity of all points in \mathcal{U}_b , resulting in a higher ρ value. Conversely, if two clusters \mathcal{U}_a and \mathcal{U}_b are not well-separated, a vector \mathbf{u}_a^\perp orthogonal to \mathcal{U}_a would likely also be orthogonal to \mathcal{U}_b , leading to small similarity and a lower ρ value. The motivation for employing *Cluster Integrity* as a metric is to maintain consistency with the attention mechanism, which calculates the affinity matrix using cosine similarity between all pairs of transformed vectors \mathbf{x}_i and \mathbf{x}_j .

Our first theoretical result, summarized in the following theorem, demonstrates that if every sample in the matrix \mathbf{X} originates from one of the defined subspaces, then the resulting affinity matrix \mathbf{A} can be theoretically constrained.

Under this constraint, samples that belong to the same class will exhibit a cosine similarity that is always greater than a polynomial function of ρ ; and samples from different classes are predicted to have a cosine similarity of 0.

Theorem 1. *Given a collection of input samples \mathbf{X} , where every sample \mathbf{x}_i comes from one subspaces among $\{\mathcal{U}_1, \dots, \mathcal{U}_K\}$, there always exists a pair of parameters $(\mathbf{W}_Q^*, \mathbf{W}_K^*)$ such that the affinity matrix \mathbf{A} calculated by (2) has a block-diagonal form, ie.*

$$\begin{cases} [\mathbf{A}]_{i,j} = 0, & \mathbf{x}_i, \mathbf{x}_j \text{ in different clusters} \\ [\mathbf{A}]_{i,j} > \nu_i \rho^2, & \mathbf{x}_i, \mathbf{x}_j \text{ in the same cluster} \end{cases}$$

where ν_i is the number of samples in same cluster as \mathbf{x}_i , and ρ is the Class Integrity defined in Definition 1.

To illustrate this, we present a simple example. Let \mathbf{X} be a matrix with $n = 4$ samples and an ambient dimension of $m = 4$:

$$\mathbf{X} = [\mathbf{x}_1^\top \quad \mathbf{x}_2^\top \quad \mathbf{x}_3^\top \quad \mathbf{x}_4^\top]^\top \in \mathbb{R}^{4 \times 4}.$$

Consider two rank-1 subspaces, $\{\mathcal{U}_1, \mathcal{U}_2\}$, where $\mathbf{x}_1, \mathbf{x}_2 \in \mathcal{U}_1$, and $\mathbf{x}_3, \mathbf{x}_4 \in \mathcal{U}_2$. The bases of these subspaces can be represented as $\{\mathbf{u}_1, \mathbf{u}_2\} \in \mathbb{R}^4$. Define:

$$\mathbf{W}^* = [\mathbf{u}_2^\perp \quad \mathbf{u}_2^\perp \quad \mathbf{u}_1^\perp \quad \mathbf{u}_1^\perp],$$

where \mathbf{u}_1^\perp and \mathbf{u}_2^\perp are bases orthogonal to \mathcal{U}_1 and \mathcal{U}_2 , respectively, i.e. $\mathbf{u}_1^\top \mathbf{u}_1^\perp = \mathbf{u}_2^\top \mathbf{u}_2^\perp = 0$. Subsequently, applying the linear transformation to matrix \mathbf{X} using \mathbf{W}^* will reveal the clustering information of the samples:

$$\mathbf{X}\mathbf{W}^* = \begin{bmatrix} \mathbf{x}_1^\top \mathbf{u}_2^\perp & \mathbf{x}_1^\top \mathbf{u}_1^\perp & 0 & 0 \\ \mathbf{x}_2^\top \mathbf{u}_2^\perp & \mathbf{x}_2^\top \mathbf{u}_1^\perp & 0 & 0 \\ 0 & 0 & \mathbf{x}_3^\top \mathbf{u}_1^\perp & \mathbf{x}_3^\top \mathbf{u}_2^\perp \\ 0 & 0 & \mathbf{x}_4^\top \mathbf{u}_1^\perp & \mathbf{x}_4^\top \mathbf{u}_2^\perp \end{bmatrix} \quad (7)$$

By setting $\mathbf{W}_K = \mathbf{W}_Q = \mathbf{W}^*$, we obtain:

$$\mathbf{A} = 2 \begin{bmatrix} (\mathbf{x}_1^\top \mathbf{u}_2^\perp)^2 & (\mathbf{x}_1^\top \mathbf{u}_1^\perp)^2 & 0 & 0 \\ (\mathbf{x}_2^\top \mathbf{u}_2^\perp)^2 & (\mathbf{x}_2^\top \mathbf{u}_1^\perp)^2 & 0 & 0 \\ 0 & 0 & (\mathbf{x}_3^\top \mathbf{u}_1^\perp)^2 & (\mathbf{x}_3^\top \mathbf{u}_2^\perp)^2 \\ 0 & 0 & (\mathbf{x}_4^\top \mathbf{u}_1^\perp)^2 & (\mathbf{x}_4^\top \mathbf{u}_2^\perp)^2 \end{bmatrix}$$

where each non-zero entry in \mathbf{A} is lower-bounded by $2\rho^2$. The proof of Theorem 1 follows without complications by generalizing this example to larger bases, more samples, and more clusters, and can be found in Appendix C.

3.2 Noisy Fusion

To address the presence of noise, the clear block-diagonal structure may not be immediately apparent within the first block. Therefore, our objective is to progressively enhance the block-diagonal nature of \mathbf{A}^ℓ with each subsequent layer ℓ . By stacking a sufficient number of layers, the final layer's output \mathbf{A}^d should possess the desired property to effectively recognizing clusters.

To achieve this objective, our initial step involves bounding the magnitude of noise. Let $\tilde{\mathbf{X}}$ denote the input data with noise such that each sample (row) of $\tilde{\mathbf{X}}$ has a non-negative cosine similarity with the corresponding sample in \mathbf{X} . And the cosine similarity is lower-bounded by a universal constant $\varepsilon \in [0, 1]$:

$$\mathbf{x}_i^\top \tilde{\mathbf{x}}_i \geq (1 - \varepsilon) \quad (8)$$

With this, we can further bound the projection of $\tilde{\mathbf{x}}_i$ onto the orthogonal complement \mathbf{u}_k^\perp :

1) When \mathbf{x}_i belongs to \mathcal{U}_k ,

$$\tilde{\mathbf{x}}_j^\top \mathbf{u}_k^\perp \leq \sqrt{(1 - (1 - \varepsilon)^2)} =: \delta$$

2) When \mathbf{x}_i does NOT belong to \mathcal{U}_k ,

$$\tilde{\mathbf{x}}_j^\top \mathbf{u}_k^\perp \geq (1 - \varepsilon)\rho - \sqrt{(1 - (1 - \varepsilon)^2)(1 - \rho^2)} =: \Delta$$

Intuitively, δ represents the similarity upperbound between the input in class k and its perpendicular vectors, and Δ represents the similarity lowerbound between the input in class k and perpendicular vectors to other class.

To validate the enhancement of cluster structure within the affinity matrix at each layer, we introduce a metric specifically devised to evaluate the similarity between matrix \mathbf{A} and an ideal block-diagonal matrix. This metric evaluates the proportion of the lowest affinity value among samples within the same class to the highest affinity value among samples from different classes. If our matrix \mathbf{A} closely resembles a block-diagonal form, this ratio is expected to approach $+\infty$, indicating a high level of class-specific clustering within the matrix.

Definition 2. The *sharpness* of an affinity matrix \mathbf{A} is defined as the infimum of the ratio between the affinity of two points within the same cluster and the affinity of two points belonging to different clusters, i.e.,

$$\mathcal{S}(\mathbf{A}) := \inf_{i,j,p,q} \frac{[\mathbf{A}]_{i,j}}{[\mathbf{A}]_{p,q}},$$

where $\mathbf{x}_i, \mathbf{x}_j$ are from the same cluster and $\mathbf{x}_p, \mathbf{x}_q$ are from different clusters.

In words, *sharpness* is quantifying how well-defined are our clusters. It bears similarity to the Silhouette index (SI) [19], commonly used for assessing cluster separation. However, a key distinction lies in the measurement approach: while SI calculates cluster quality using average distances for both intra-cluster and inter-cluster sample pairs, the *sharpness* metric evaluates the ratio of the maximum intra-cluster distance to the minimum inter-cluster distance, and thus, imposes more stringent requirements on the structural integrity of the clusters.

Building upon this foundation, we substantiate that, mirroring the configuration of noise-free data, every *TransFusion* block possesses the capacity to enhance the **sharpness** of its affinity matrix compared to the preceding layer. This enhancement is quantifiable by a constant factor determined by δ, Δ , and batch size n .

Theorem 2. Given a input matrix $\tilde{\mathbf{X}}$, where each sample $\tilde{\mathbf{x}}_i$ lies near one of the subspaces among $\{\mathcal{U}_1, \dots, \mathcal{U}_K\}$ with noise bounded by (8), there always exists a pair of parameter $(\mathbf{W}_Q^*, \mathbf{W}_K^*)$ such that each *TransFusion* block

increases the **sharpness** of its similarity matrix \mathbf{A}^ℓ by at least a factor of $\gamma := \frac{(\Delta^3 - n^2(\delta + \delta^2))^2(2 + \delta)}{\Delta^2 n^3 (\Delta^2 + (1 + \delta))(1 + \delta(\Delta^2 + (1 + \delta)))}$.

Theorem 2 conveys that the sharpness of similarity matrix is proportional to $\mathbf{O}(\Delta^2 n)$, which can be further simplifies to $\mathbf{O}((1 - \varepsilon)^2 \rho^2 n)$. This implies that having low noise, isolated clusters, and large number of samples are the major factor that determine a successful fusion process. This observation is consistent with general findings in the field of contrastive learning [1, 13]. This will ultimately lead to an enhanced block-diagonal pattern within the similarity matrix \mathbf{A} .

The proof of Theorem 2 follows by the same arguments as that of Theorem 1, except the off-diagonal blocks are upper bounded by δ instead of zero, and the diagonal blocks are lower bounded by Δ . The detailed proof can be found in the Appendix D. Moreover, through numerical experiments, we depict the feasible learning area for the pair (ρ, ε) under varying batch sizes. This area guarantees that the *sharpness* increment γ is greater than 1. The detailed results are presented in Figure 2

4 Related Work

This section reviews two major areas of recent research relevant to *TransFusion*. The first part examines the latest advancements in contrastive learning, dividing the discussion into self-supervised and supervised methods. The second part evaluates how *TransFusion* relates to other models that are based on attention mechanisms.

4.1 Contrast Learning

In the domain of contrastive learning, each individual image is treated as a distinct class, and the model is honed to discern augmented versions of the same image amidst a backdrop of other images. Approaches conceived within this category conventionally revolve around designating an anchor image and then generating augmentations of this anchor image. In tandem with the other images, the model is instructed to intensify the similarity between the anchor image and its augmentations, while concurrently diminishing the similarity between the anchor image and the remaining images. A noteworthy milestone emerges in the form of a seminal study conducted by [5]. This work introduces a non-parametric approach for gauging the similarity between features, thereby elevating accuracy levels across datasets

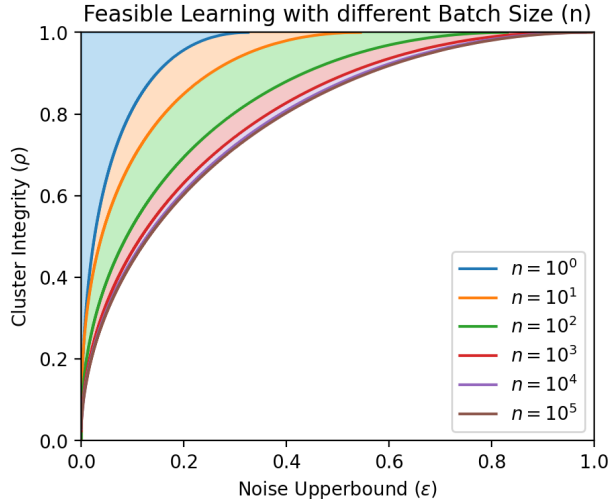


Figure 2: Numerical validation of Theorem 2. Each line represents the minimum learning requirement (*sharpness* increment $\gamma > 1$) for a specific batch size (n). The shaded area further signifies the fusion area’s effectiveness, where the (ρ, ε) pair adheres to more lenient conditions.

like CIFAR10 and ImageNet. Another significant contribution comes from [20], who showcase the potential of maximizing mutual information between an input and the output of a neural network encoder. Similarly, [2] build upon a comparable method to amplify the mutual information across diverse channels of a scene’s view. The results of their experimentation corroborate the efficacy of this approach. Intriguingly, the utilization of contrastive learning has ushered in a remarkable shift in training larger networks with significantly fewer labeled data points, all the while achieving competitive outcomes on prominent datasets such as Imagenet [1] and PASCAL VOC [6]. A more recent contribution that stands out is the work undertaken by [21]. Remarkably, this study unveils the closed-form optimal representation and network parameters within the linear regime for prevalent self-supervised learning approaches, including VICReg [3], SimCLR [1], and BarlowTwins [4].

Contrastive Learning finds its application not only within unsupervised settings but also extends its influence to supervised learning. Rather than treating each image as an isolated class, this approach takes advantage of the labels by encouraging comparisons between images spanning various classes. The goal is to minimize the distance between embeddings belonging to the same class. One notable contribution in this direction, presented by [22], demonstrates that by pairing images from the same class as the anchor image, the model exhibits enhanced performance across datasets such as CIFAR10 and CIFAR100. [23] propose an innovative methodology encompassing a dual-pronged approach. They employ a network to grasp the nuances of the discriminative task, complemented by a graph-based model that effectively brings together similar samples. Addressing the challenge of imbalanced class label distributions, [17] introduce a novel model called Parametric Contrastive Learning (PaCo). This model not only tackles the issue but also establishes itself as a leader in the domain of long-tailed recognition. In the domain of few-shot embedding model training, [24] delve into the combination of contrastive learning with Noise Contrastive Estimation (NCE) within a supervised framework. This strategic integration leads to commendable performance on the mini-ImageNet dataset.

4.2 Attention-Based Models

In the realm of Transformers, the substitution of the Softmax function with ReLU was initially explored in a study by [25]. They introduced *ReLUFormer*, with a primary focus on language tasks. Their findings showed that ReLU outperforms Softmax in managing long sequence tasks within the Transformer framework, attributing *ReLUFormer*’s enhanced expressiveness to its higher variance compared to Softmax. This observation is consistent with our ablation studies in the field of contrastive learning. [26] proposed *BatchFormer*, a model sharing similarities with *TransFusion*. *BatchFormer* leverages the Transformer architecture to learn relationships between samples in a mini-batch. This approach enables collaborative learning among different samples within a mini-batch, proving especially beneficial in complex scenarios such as long-tailed recognition. However, what distinguishes *TransFusion* structurally is its training process that learns embeddings based on the affinity matrix instead of labels, which eliminates the need for a classifier and thereby facilitates both supervised and self-supervised contrastive learning. Moreover, unlike

BatchFormer, *TransFusion* offers theoretical insights and assurances for achieving successful outcomes in contrastive learning.

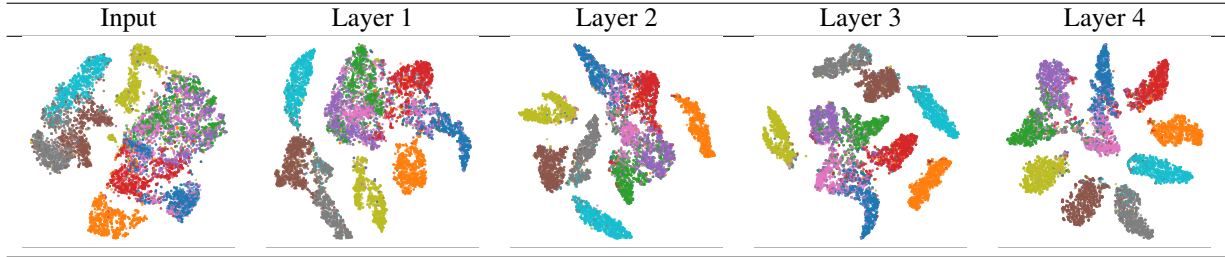


Figure 4: Fusion Effect of the 5-layer *TransFusion* trained on FashionMNIST through unsupervised contrastive learning. We extract the output from each *TransFusion* block and visualize it using t-SNE. As we progress through deeper layers, it is observed that the clusters become more condensed and exhibit reduced noise at the boundaries.

5 Experiment

In this section, we showcase the practical effectiveness of *TransFusion* through a series of experiments on real-world datasets. We begin by illustrating *TransFusion*'s layer-by-layer fusion process using the FashionMNIST dataset. This is done by visualizing the embeddings from each layer using t-Distributed Stochastic Neighbor Embedding (t-SNE) [27], a technique that effectively reduces high-dimensional data to a lower-dimensional space while maintaining the data's inherent relationships and structure. As we progress through the deeper layers, we observe a clear and successful fusion process, evidenced by the increasingly distinct and denser clustering of data points.

Subsequently, we present empirical training results using the CIFAR10 dataset, applying both self-supervised and supervised learning approaches. In our analysis, we compare the fine-tuning accuracy of *TransFusion* with other leading methods in contrastive learning. The results highlight *TransFusion*'s superior performance, emphasizing its efficacy and potential in deep learning applications. Pytorch implementations for all experiments can be found in Appendix E.

5.1 Visualizing *TransFusion*'s Fusion Process

TransFusion operates on the fundamental concept of utilizing attention mechanisms to modify the embedding space, resulting in closer distances between related objects and farther distances between non-related objects. Through this fusion process, clusters become more concentrated and isolated, leading to enhanced distinctiveness among individual clusters. As demonstrated in the previous section, our theoretical framework establishes the result that each layer in the model should consistently amplify the overall cluster structure. In this section, we substantiate this claim through empirical experiments conducted on real-world datasets.

To provide a visual representation of the fusion's influence, we build a 5-layer *TransFusion* model for the fashion-MNIST datasets. Each layer takes the input of dimension 784 and has learnable weight matrices $\mathbf{W}_Q, \mathbf{W}_K, \mathbf{W}_V \in \mathbb{R}^{784 \times 784}$. For training, we utilize Adam optimizers and conduct 200 epochs with learning rate 0.1. Following the training phase, we evaluate the models using unseen test datasets, and we extract intermediate outputs from each layer to generate embeddings through t-SNE. The results obtained from this process are presented in Figure 4.

On the left-hand side of each graph, we observe the initial embeddings derived directly from the data. As we move from left to right within each row, we showcase embeddings from layers that are deeper into the models. In these graphs, each distinct class is delineated by a unique color, and this color scheme is consistently maintained across the respective datasets. Upon analyzing the graphs, we observed that, with increasing depth, the clusters demonstrate enhanced separation, and become more condensed, with a noticeable reduction in noise at their boundaries. These phenomena contribute to the enhancement of the *sharpness* in the affinity matrix. These observations are in concordance with the theoretical framework of *TransFusion*, which suggests that each successive layer contributes to refining the sharpness of the affinity matrix.

5.2 Empirical Results on CIFAR10

In this section, we initiate a detailed empirical comparison, contrasting our methodology with other contemporary advancements focusing on infoNCE loss functions. Throughout the experiments detailed in this section, we adopt

Model	Batch Size	3-FFN	SVM	K-NN (k=50)	K-NN (k=200)	Time (min)
InfoNCE	128	0.3854	0.3728	0.3398	0.32	990
DCL	128	0.3736	0.383	0.3099	0.2962	705
BarlowTwins	128	0.4827	0.5032	0.4259	0.4085	752
TransFusion 1-Layer	128	0.5231	0.5102	0.4231	0.4107	764
TransFusion 9-Layer	128	0.5626	0.5430	0.4616	0.4453	706

Table 1: Self-Supervised classification accuracy (0-1) for CIFAR-10 Using SimpCLR with different loss functions. Each model was trained with ResNet18 as the underlying architecture, underwent a 200-epoch training process, and fined-tuned with 100% labels.

Model	Batch Size	3-FFN	SVM	K-NN (k=50)	K-NN (k=200)	Time (min)
SupCon	128	0.8121	0.8049	0.7907	0.7717	352
SupCon	1024	0.9091	0.9056	0.9002	0.8931	641
TransFusion 1-Layer	128	0.9475	0.9309	0.9355	0.9350	368
TransFusion 9-Layer	128	0.9489	0.9432	0.9487	0.9487	380
ResNet-18	128	0.935	-	-	-	-

Table 2: Fully-Supervised classification accuracy (0-1) for CIFAR-10 Using SimpCLR with different loss functions. Each model was trained with ResNet18 as the underlying architecture and underwent a 200-epoch training process.

SimpCLR [1] as our foundational framework for contrastive learning. Specifically, SimpCLR employs a singular backbone network to assess similarities within batch samples. Our backbone model is an 18-layer ResNet, as described in [28]. The fully-connected layer of ResNet-18 is replaced with a flatten layer to extract embeddings. Subsequently, we train the model using a variety of loss functions to evaluate their performance.

After the training phase, we extract the intermediate outputs (size 512) from the ResNet backbone. These outputs, functioning as embeddings, are then harnessed to train a 3-layer feed-forward network, having layer widths of 256, 128, and 64, respectively. Moreover, we incorporate the use of a Support Vector Machine (SVM) [29] and K-Nearest-Neighbor (K-NN), training it with the embeddings generated from the training set, as suggested by [30, 13]. We then proceed to apply the model for classification tasks on the embeddings derived from the test dataset.

5.2.1 Self-Supervised Learning

In this section, our focus is on benchmarking our model against a variety of other self-supervised models, each offering advancements on the InfoNCE loss function. For our experiments, we utilize straightforward image augmentations to enhance the training process. These augmentations include 1) Random Crop, with a scale range of (0.8, 1), and 2) Color Jitter, characterized by settings of brightness = 0.2, contrast = 0.2, saturation = 0.2, hue = 0.1. Following the initial phase of contrastive learning, we fine-tune a final 3-layer Feed-Forward Network (FFN) using the entire label set. This step primarily aims to explore the maximum potential performance that each loss function can achieve.

The loss functions selected for this comparative study include the InfoNCE [31], Decoupled Contrastive Learning loss (DCL) [13], BarlowTwins [4]. To ensure a level playing field, a 1-layer TransFusion model serves as our standard benchmark to avoid the confounding effects of additional learnable parameters. Nevertheless, we also report the peak results from a more complex 9-layer TransFusion model. Both variations construct weight matrices $\mathbf{W}_Q, \mathbf{W}_K, \mathbf{W}_V \in \mathbb{R}^{512 \times 512}$. The 1-layer TransFusion model introduces fewer than 0.5M parameters, while the 9-layer model adds an additional 7M parameters.

The results, as summarized in Table 1, highlight the competitive edge of the TransFusion approach in the self-supervised learning landscape. The 1-layer TransFusion model not only surpasses its contemporaries in performance but does so with a minimal increase in computational time. This efficacy is even more pronounced in the 9-layer TransFusion model, which achieves the highest overall performance in the comparison. Notably, these improvements in performance are attained without a proportional increase in training time.

5.2.2 Supervised Learning

In this section, we compare our approach with the Supervised Contrastive Learning method referred to as *SupCon* [22]. *SupCon* essentially represents a modified variant of *InfoNCE*, but with the incorporation of supervised labels. This implies that, within each batch, images belonging to the same class are expected to exhibit high similarity, while

those from different classes should display minimal similarity. Our backbone for both methods are pre-trained on the ImageNet1K dataset.

For this experiment, we did not introduce any augmentation techniques. To enhance training performance, the input images were resized from dimensions of (32, 32, 3) to (224, 224, 3). The results in Table 2 clearly indicate that *TransFusion* consistently outperforms *SupCon*, even when *SupCon* is trained with a larger batch size—a practice commonly thought to be more effective for contrastive learning, as noted in [1]. Remarkably, *ResNet18* achieves an accuracy of 0.935 when trained with full labels using cross-entropy loss in our own experiment. This underscores that 1-layer *TransFusion* achieves even better performance to a fully-supervised model.

6 Conclusion & Future Direction

In this paper, we introduced *TransFusion*, a novel framework for training attention-based neural networks for contrastive learning. Our theoretical analysis demonstrates that each layer in the *TransFusion* contributes to the fusion process, enhancing the embedding space’s density and distinctiveness across different classes. Through experiments, we validated the efficacy of *TransFusion* by showcasing its ability with its superior classification accuracies in both supervised and unsupervised settings.

References

- [1] T. Chen, S. Kornblith, M. Norouzi, and G. Hinton, “A simple framework for contrastive learning of visual representations,” in *International conference on machine learning*. PMLR, 2020, pp. 1597–1607. 1, 6, 7, 9, 10
- [2] Y. Tian, D. Krishnan, and P. Isola, “Contrastive multiview coding,” in *Computer Vision—ECCV 2020: 16th European Conference, Glasgow, UK, August 23–28, 2020, Proceedings, Part XI 16*. Springer, 2020, pp. 776–794. 1, 7
- [3] A. Bardes, J. Ponce, and Y. LeCun, “Vicreg: Variance-invariance-covariance regularization for self-supervised learning,” *arXiv preprint arXiv:2105.04906*, 2021. 1, 7
- [4] J. Zbontar, L. Jing, I. Misra, Y. LeCun, and S. Deny, “Barlow twins: Self-supervised learning via redundancy reduction,” in *International Conference on Machine Learning*. PMLR, 2021, pp. 12 310–12 320. 1, 7, 9
- [5] Z. Wu, Y. Xiong, S. X. Yu, and D. Lin, “Unsupervised feature learning via non-parametric instance discrimination,” in *Proceedings of the IEEE conference on computer vision and pattern recognition*, 2018, pp. 3733–3742. 1, 6, 12
- [6] O. Henaff, “Data-efficient image recognition with contrastive predictive coding,” in *International conference on machine learning*. PMLR, 2020, pp. 4182–4192. 1, 7
- [7] A. Jaiswal, A. R. Babu, M. Z. Zadeh, D. Banerjee, and F. Makedon, “A survey on contrastive self-supervised learning,” *Technologies*, vol. 9, no. 1, p. 2, 2020. 1
- [8] X. Wang and G.-J. Qi, “Contrastive learning with stronger augmentations,” *IEEE transactions on pattern analysis and machine intelligence*, vol. 45, no. 5, pp. 5549–5560, 2022. 1
- [9] N. Saunshi, J. Ash, S. Goel, D. Misra, C. Zhang, S. Arora, S. Kakade, and A. Krishnamurthy, “Understanding contrastive learning requires incorporating inductive biases,” in *International Conference on Machine Learning*. PMLR, 2022, pp. 19 250–19 286. 1
- [10] Y. Tian, C. Sun, B. Poole, D. Krishnan, C. Schmid, and P. Isola, “What makes for good views for contrastive learning?” *Advances in neural information processing systems*, vol. 33, pp. 6827–6839, 2020. 1
- [11] T. Xiao, X. Wang, A. A. Efros, and T. Darrell, “What should not be contrastive in contrastive learning,” *arXiv preprint arXiv:2008.05659*, 2020. 1
- [12] Y. Wang, Q. Zhang, Y. Wang, J. Yang, and Z. Lin, “Chaos is a ladder: A new theoretical understanding of contrastive learning via augmentation overlap,” *arXiv preprint arXiv:2203.13457*, 2022. 1
- [13] C.-H. Yeh, C.-Y. Hong, Y.-C. Hsu, T.-L. Liu, Y. Chen, and Y. LeCun, “Decoupled contrastive learning,” in *European Conference on Computer Vision*. Springer, 2022, pp. 668–684. 1, 6, 9
- [14] J. Yang, C. Li, P. Zhang, B. Xiao, C. Liu, L. Yuan, and J. Gao, “Unified contrastive learning in image-text-label space,” in *Proceedings of the IEEE/CVF Conference on Computer Vision and Pattern Recognition*, 2022, pp. 19 163–19 173. 1

- [15] J. Yang, J. Duan, S. Tran, Y. Xu, S. Chanda, L. Chen, B. Zeng, T. Chilimbi, and J. Huang, “Vision-language pre-training with triple contrastive learning,” in *Proceedings of the IEEE/CVF Conference on Computer Vision and Pattern Recognition*, 2022, pp. 15 671–15 680. [1](#)
- [16] J. Zhu, Z. Wang, J. Chen, Y.-P. P. Chen, and Y.-G. Jiang, “Balanced contrastive learning for long-tailed visual recognition,” in *Proceedings of the IEEE/CVF Conference on Computer Vision and Pattern Recognition*, 2022, pp. 6908–6917. [1](#)
- [17] J. Cui, Z. Zhong, S. Liu, B. Yu, and J. Jia, “Parametric contrastive learning,” in *Proceedings of the IEEE/CVF international conference on computer vision*, 2021, pp. 715–724. [1](#), [7](#)
- [18] S. Kullback and R. A. Leibler, “On information and sufficiency,” *The annals of mathematical statistics*, vol. 22, no. 1, pp. 79–86, 1951. [4](#)
- [19] P. J. Rousseeuw, “Silhouettes: a graphical aid to the interpretation and validation of cluster analysis,” *Journal of computational and applied mathematics*, vol. 20, pp. 53–65, 1987. [6](#)
- [20] R. D. Hjelm, A. Fedorov, S. Lavoie-Marchildon, K. Grewal, P. Bachman, A. Trischler, and Y. Bengio, “Learning deep representations by mutual information estimation and maximization,” *arXiv preprint arXiv:1808.06670*, 2018. [7](#)
- [21] R. Balestriero and Y. LeCun, “Contrastive and non-contrastive self-supervised learning recover global and local spectral embedding methods,” *Advances in Neural Information Processing Systems*, vol. 35, pp. 26 671–26 685, 2022. [7](#)
- [22] P. Khosla, P. Teterwak, C. Wang, A. Sarna, Y. Tian, P. Isola, A. Maschinot, C. Liu, and D. Krishnan, “Supervised contrastive learning,” *Advances in neural information processing systems*, vol. 33, pp. 18 661–18 673, 2020. [7](#), [9](#), [12](#)
- [23] M. Zheng, F. Wang, S. You, C. Qian, C. Zhang, X. Wang, and C. Xu, “Weakly supervised contrastive learning,” in *Proceedings of the IEEE/CVF International Conference on Computer Vision*, 2021, pp. 10 042–10 051. [7](#)
- [24] C. Liu, Y. Fu, C. Xu, S. Yang, J. Li, C. Wang, and L. Zhang, “Learning a few-shot embedding model with contrastive learning,” in *Proceedings of the AAAI conference on artificial intelligence*, vol. 35, no. 10, 2021, pp. 8635–8643. [7](#)
- [25] K. Shen, J. Guo, X. Tan, S. Tang, R. Wang, and J. Bian, “A study on relu and softmax in transformer,” *arXiv preprint arXiv:2302.06461*, 2023. [7](#)
- [26] Z. Hou, B. Yu, and D. Tao, “Batchformer: Learning to explore sample relationships for robust representation learning,” in *Proceedings of the IEEE/CVF Conference on Computer Vision and Pattern Recognition*, 2022, pp. 7256–7266. [7](#)
- [27] L. Van der Maaten and G. Hinton, “Visualizing data using t-sne,” *Journal of machine learning research*, vol. 9, no. 11, 2008. [8](#)
- [28] K. He, X. Zhang, S. Ren, and J. Sun, “Deep residual learning for image recognition,” in *Proceedings of the IEEE conference on computer vision and pattern recognition*, 2016, pp. 770–778. [9](#), [12](#), [13](#)
- [29] M. A. Hearst, S. T. Dumais, E. Osuna, J. Platt, and B. Scholkopf, “Support vector machines,” *IEEE Intelligent Systems and their applications*, vol. 13, no. 4, pp. 18–28, 1998. [9](#), [12](#)
- [30] J. Li, P. Zhou, C. Xiong, and S. C. Hoi, “Prototypical contrastive learning of unsupervised representations,” *arXiv preprint arXiv:2005.04966*, 2020. [9](#), [12](#)
- [31] A. v. d. Oord, Y. Li, and O. Vinyals, “Representation learning with contrastive predictive coding,” *arXiv preprint arXiv:1807.03748*, 2018. [9](#)

A Appendix: Relation to InfoNCE

In this section, we demonstrate its relationship with well-known InfoNCE [5] in both self-supervised and supervised manner. Specifically, for self-supervised learning, InfoNCE can be found in the form of:

$$\mathcal{L}_{\text{self}} = - \sum_{i \in I} \log \frac{\exp(\mathbf{z}_i^\top \mathbf{z}_{j(i)}/\tau)}{\sum_{i \neq a} \exp(\mathbf{z}_i^\top \mathbf{z}_b/\tau)} \quad (9)$$

where I denote the collection of samples from the current training batch; τ is a temperature constant; \mathbf{z}_i is the feature extracted from i 'th sample; $j(i)$ corresponding to the positive example of sample i , which is usually generated by augmentation of sample i .

Since it's self-supervised learning, we know that there only exit 1 positive sample for each batch, which means that $|P(i)| = 1$, and $[\mathbf{Y}]_{ij}$ can only be either 0 or 1. This means that the loss can be simplified to:

$$\mathcal{L}_{\text{TF}} := \mathcal{D}(\mathbf{Y} || \sigma(\mathbf{A}^d/\tau)) = \sum_{i,j} [\mathbf{Y}]_{i,j} \log \frac{[\mathbf{Y}]_{i,j}}{[\sigma(\mathbf{A}^d/\tau)]_{i,j}} = \sum_{i \in I, j \in P(i)} -\log [\sigma(\mathbf{A}^d/\tau)]_{i,j}.$$

If we force the weight of Key and Query in the last layer to be the same $\mathbf{W}_Q^d = \mathbf{W}_K^d = \tilde{\mathbf{W}}$, then we can have embeddings \mathbf{Z} denote as: $\mathbf{Z} := \mathbf{X}^\ell \tilde{\mathbf{W}}$, and

$$[\sigma(\mathbf{A}^d/\tau)]_{i,j} = \frac{\exp(\mathbf{z}_i^\top \mathbf{z}_j/\tau)}{\sum_{i \neq a} \exp(\mathbf{z}_i^\top \mathbf{z}_b/\tau)}$$

which is exactly the same as $\mathcal{L}_{\text{self}}$.

For supervised learning manner, referring to [22], the loss can be defined as

$$\mathcal{L}_{\text{sup}} = \sum_{i \in I} \frac{-1}{|P(i)|} \sum_{p \in P(i)} \log \frac{\exp(\mathbf{z}_i^\top \mathbf{z}_p/\tau)}{\sum_{a \neq i} \exp(\mathbf{z}_i^\top \mathbf{z}_b/\tau)} \quad (10)$$

where $P(i)$ denote the collection of samples from the same class as i 'th sample. By plugging in (1) to (4), it's trivial that $\mathcal{L}_{\text{sup}} = \mathcal{L}_{\text{TF}}$.

B Appendix: Ablation Studies of Different Loss Functions

In this section, we undertake an empirical comparison among different loss functions. To conduct this comparison, we used CIFAR10 and trained a one-layer Transfusion model on top of a pretrained 18 Layer ResNet [28], employing each of the loss functions separately. Subsequently, we extracted the intermediate output from the ResNet as embeddings. These embeddings were then utilized to train a Support Vector Machine [29] on the training dataset, followed by performing classification on the embeddings from the test dataset. This procedure is a standard practice for evaluating the quality of the fixed embeddings, aligning with the recommendation provided by [30].

The Transfusion's training process follows a supervised contrastive learning approach, where the target affinity matrix is constructed based on the class labels of the samples. For this experiment, we did not introduce any augmentation techniques. To enhance training performance, the input images were resized from dimensions of (32, 32, 3) to (224, 224, 3).

Recall that one layer Transfusion model is essentially generating the cosine similarity between samples:

$$\mathbf{A} := (\mathbf{Z}\mathbf{W}_Q)(\mathbf{Z}\mathbf{W}_K)^\top \quad (11)$$

where $\mathbf{Z} \in \mathbb{R}^{n \times m}$ denotes the embeddings from the upstream ResNet18 model; n denotes the number of samples; m denotes the ambient dimension; $\mathbf{W}_Q, \mathbf{W}_K \in \mathbb{R}^{m \times m}$ denotes learn-able parameters. The loss functions we are interested are:

- Supervised InfoNCE (KL-Divergence with Softmax) (10): $\mathcal{L}_{\text{KL-Softmax}} := \mathcal{D}(\mathbf{Y} || \sigma(\mathbf{A}))$
- KL-Divergence with ReLU (KL-ReLU): $\mathcal{L}_{\text{KL-ReLU}} := \mathcal{D}(\mathbf{Y} || \text{Normalize}(\mathbf{A}_+))$
- KL-Divergence with Squared Affinity (KL-Squared): $\mathcal{L}_{\text{KL-Squared}} := \mathcal{D}(\mathbf{Y} || \text{Normalize}(\mathbf{A}^2))$

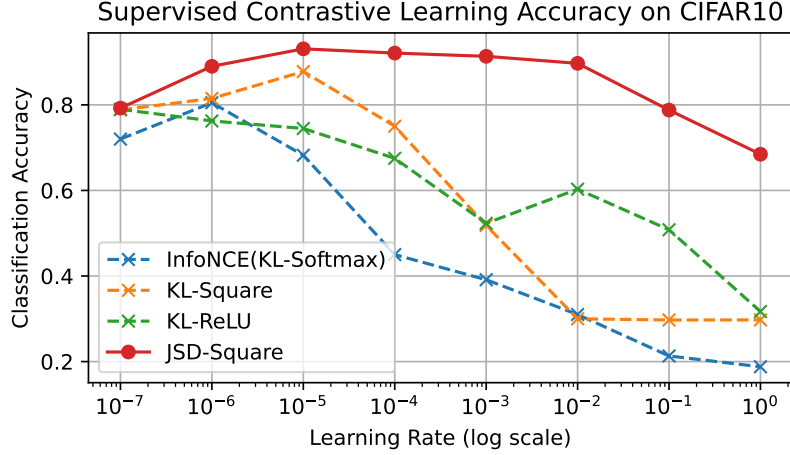


Figure 5: Precision in the encoding derived from a single-layer Transfusion model on top of ResNet18 [28] with supervised contrastive learning. This experiment was conducted on the CIFAR10 dataset, with ResNet18 pretrained on ImageNet1K as the underlying model.

- Jensen-Shannon Divergence with Squared Affinity (JSD-Squared):

$$\mathcal{L}_{\text{JSD-Squared}} := \mathcal{D}(\mathbf{Y} \parallel \text{Normalize}(\mathbf{A}^2)/2 + \mathbf{Y}/2) + \mathcal{D}(\text{Normalized}(\mathbf{A}^2) \parallel \text{Normalize}(\mathbf{A}^2)/2 + \mathbf{Y}/2)$$

The outcomes for each of the loss functions are depicted in Figure 5. From the results, it is evident that our custom loss function exhibits remarkable robustness across a broad spectrum of learning rates. It consistently maintains stable regions where classification accuracy remains consistently high. The next best performer is the KL-Squared, which shares similarities with the JSD-Squared. Notably, there are slight improvements when opting for JSD over KL. In contrast, it becomes apparent that the KL-Softmax function displays a heightened sensitivity to variations in the learning rate. Across numerous trials, we encountered challenges such as overflows, even after normalizing the values prior to the Softmax operation.

C Appendix: Proof of Theorem 1

In words, Theorem 1 shows that the linear transformation of \mathbf{x}_i and \mathbf{x}_j has a cosine similarity of zero if they are from different clusters, and a positive similarity with lower bound if they belong to the same cluster. What follows is a detailed proof of this theorem.

Proof. Consider a matrix $\mathbf{X} \in \mathbb{R}^{n \times m}$, representing n samples each in an m -dimensional ambient space. These samples are partitioned into C clusters. Let c_i denote the cluster assignment for the sample \mathbf{x}_i , where $c_i \in \{1, 2, \dots, C\}$.

Introduce a weight matrix $\mathbf{W} \in \mathbb{R}^{m \times n}$, where each column \mathbf{w}_i is constructed to be orthogonal to the subspaces corresponding to all clusters except the one containing \mathbf{x}_i .

Consequently, the product \mathbf{XW} yields:

$$[\mathbf{XW}]_{i,j} = \mathbf{x}_i^\top \mathbf{w}_j = \begin{cases} 0 & \text{if } c_i \neq c_j, \\ \geq \rho & \text{if } c_i = c_j, \end{cases}$$

where ρ is a predefined lower bound.

For any pair of samples $\mathbf{x}_i, \mathbf{x}_j$ in the same cluster, the i -th and j -th rows of \mathbf{XW} , denoted as $[\mathbf{XW}]_{i,\cdot}$ and $[\mathbf{XW}]_{j,\cdot}$, respectively, have coinciding non-zero entry locations. Therefore,

$$[\mathbf{A}]_{i,j} = [\mathbf{XW}]_{i,\cdot}^\top [\mathbf{XW}]_{j,\cdot} \geq \nu_i \rho^2, \quad (12)$$

where ν_i is the number of samples in the same cluster as \mathbf{x}_i .

Conversely, for any pair of samples $\mathbf{x}_i, \mathbf{x}_j$ belonging to different clusters, the non-zero entry locations in the i -th and j -th rows of \mathbf{XW} are entirely distinct. Thus,

$$[\mathbf{A}]_{i,j} = [\mathbf{XW}]_{i,\cdot}^\top [\mathbf{XW}]_{j,\cdot} = 0. \quad (13)$$

□

D Appendix: Proof of Theorem 2

Proof. Our proof of Theorem 2 will apply to our construction without the residual connection. The proof with residual connection follows the same logistic. Recall that

- The cosine similarity between noisy and original sample is lower-bounded by a universal constant $\varepsilon \in [0, 1]$:

$$\mathbf{x}_i^\top \tilde{\mathbf{x}}_i \geq (1 - \varepsilon)$$

- When \mathbf{x}_i is in the span of \mathbf{u}

$$\tilde{\mathbf{x}}_i^\top \mathbf{u}^\perp \leq \sqrt{(1 - (1 - \varepsilon)^2)} := \delta$$

- When \mathbf{x}_i is not in the span of \mathbf{u} ,

$$\tilde{\mathbf{x}}_i^\top \mathbf{u}^\perp \geq (1 - \varepsilon)\rho - \sqrt{(1 - (1 - \varepsilon)^2)(1 - \rho^2)} := \Delta$$

Consider a matrix $\mathbf{X} \in \mathbb{R}^{n \times m}$, representing n samples each in an m -dimensional ambient space. These samples are partitioned into C clusters. Let c_i denote the cluster assignment for the sample \mathbf{x}_i , where $c_i \in \{1, 2, \dots, C\}$.

Introduce a weight matrix $\mathbf{W} \in \mathbb{R}^{m \times n}$, where each column \mathbf{w}_i is constructed to be orthogonal to the subspaces corresponding to all clusters except the one containing \mathbf{x}_i .

Consequently, the product $\tilde{\mathbf{X}}\mathbf{W}$ yields:

$$[\tilde{\mathbf{X}}\mathbf{W}]_{i,j} = \tilde{\mathbf{x}}_i^\top \mathbf{w}_j = \begin{cases} \leq \delta & \text{if } c_i \neq c_j, \\ \geq \Delta & \text{if } c_i = c_j. \end{cases}$$

For any pair of samples $\tilde{\mathbf{x}}_i, \tilde{\mathbf{x}}_j$ in the same cluster, the i -th and j -th rows of $\tilde{\mathbf{X}}\mathbf{W}$, denoted as $[\tilde{\mathbf{X}}\mathbf{W}]_{i,\cdot}$ and $[\tilde{\mathbf{X}}\mathbf{W}]_{j,\cdot}$, respectively, have coinciding non-zero entry locations. Therefore,

$$[\mathbf{A}]_{i,j} = [\tilde{\mathbf{X}}\mathbf{W}]_{i,\cdot}^\top [\tilde{\mathbf{X}}\mathbf{W}]_{j,\cdot} \geq \nu_i \Delta^2 := \alpha, \quad (14)$$

where ν_i is the number of samples in the same cluster as $\tilde{\mathbf{x}}_i$.

Conversely, for any pair of samples $\tilde{\mathbf{x}}_i, \tilde{\mathbf{x}}_j$ belonging to different clusters, the non-zero entry locations in the i -th and j -th rows of $\tilde{\mathbf{X}}\mathbf{W}$ are entirely distinct. Thus,

$$[\mathbf{A}]_{i,j} = [\tilde{\mathbf{X}}\mathbf{W}]_{i,\cdot}^\top [\tilde{\mathbf{X}}\mathbf{W}]_{j,\cdot} \leq (\nu_i + \nu_j)\delta + (n - \nu_i - \nu_j)\delta^2 := \beta \quad (15)$$

Denote $\tilde{\mathbf{x}}'_i$ the input of the next layer corresponding to $\tilde{\mathbf{x}}_i$, then for the worst case, we have

$$\tilde{\mathbf{x}}'_i = \sum_{c_j=c_i} \alpha \tilde{\mathbf{x}}_j + \sum_{c_k \neq c_i} \beta \tilde{\mathbf{x}}_k$$

Then,

- When $\tilde{\mathbf{x}}'_i$ is in the span of \mathbf{u} ,

$$\tilde{\mathbf{x}}'_i{}^\top \mathbf{u}^\perp = \alpha \sum_{c_j=c_i} \tilde{\mathbf{x}}_j^\top \mathbf{u}^\perp + \beta \sum_{c_k \neq c_i} \tilde{\mathbf{x}}_k^\top \mathbf{u}^\perp \leq \alpha \nu_i \delta + \beta(n - \nu_i)$$

- When $\tilde{\mathbf{x}}'_i$ is not in the span of \mathbf{u} ,

$$\tilde{\mathbf{x}}'_i{}^\top \mathbf{u}^\perp = \alpha \sum_{c_j=c_i} \tilde{\mathbf{x}}_j^\top \mathbf{u}^\perp + \beta \sum_{c_k \neq c_i} \tilde{\mathbf{x}}_k^\top \mathbf{u}^\perp \geq \alpha \nu_i \Delta - \beta(n - \nu_i)$$

Thus, for the affinity of next layer \mathbf{A}'

$$[\mathbf{A}']_{i,j} = \begin{cases} \geq \nu_i (\alpha \nu_i \Delta - \beta(n - \nu_i))^2, & c_i = c_j \\ \leq (\nu_i + \nu_j) (\alpha \nu_i \delta + \beta(n - \nu_i)) + (n - \nu_i - \nu_j) (\alpha \nu_i \delta + \beta(n - \nu_i))^2, & c_i \neq c_j \end{cases}$$

With further simplification,

$$[\mathbf{A}']_{i,j} = \begin{cases} \geq (\Delta^3 - n^2(\delta + \delta^2))^2, & c_i = c_j \\ \leq n(n^2\Delta^2\delta + n^2(\delta + \delta^2)) + n(n^2\Delta^2\delta + n^2(\delta + \delta^2))^2, & c_i \neq c_j \end{cases}$$

Recall Definition 2 that the **sharpness** of the similarity score matrix S is defined as the infimum of the ratio between the similarity scores of two points within the same cluster and the similarity scores of two points belonging to different clusters.

$$\mathcal{D}(S) := \inf_{i,j,k,h} \frac{S_{i,j}}{S_{k,h}}$$

where x_i, x_j are from the same cluster and x_k, x_h are from different clusters.

That means that

$$\begin{aligned} \mathcal{D}(S) &= \frac{\alpha}{\beta} \leq \frac{\Delta^2}{2\delta + \delta^2} \\ \mathcal{D}(S') &= \frac{(\Delta^3 - n^2(\delta + \delta^2))^2}{n(n^2\Delta^2\delta + n^2(\delta + \delta^2)) + n(n^2\Delta^2\delta + n^2(\delta + \delta^2))^2} \end{aligned}$$

Thus, the ratio of sharpness increased by next layer is:

$$\begin{aligned} \frac{\mathcal{D}(S')}{\mathcal{D}(S)} &\geq \frac{(\Delta^3 - n^2(\delta + \delta^2))^2 (2\delta + \delta^2)}{\Delta^2 n(n^2\Delta^2\delta + n^2(\delta + \delta^2)) + \Delta^2 n(n^2\Delta^2\delta + n^2(\delta + \delta^2))^2} \\ &\geq \frac{(\Delta^3 - n^2(\delta + \delta^2))^2 (2 + \delta)}{\Delta^2 n(n^2\Delta^2 + n^2(1 + \delta)) + \Delta^2 n\delta(n^2\Delta^2 + n^2(1 + \delta))^2} \\ &\geq \frac{(\Delta^3 - n^2(\delta + \delta^2))^2 (2 + \delta)}{\Delta^2 n^3(\Delta^2 + (1 + \delta)) + \Delta^2 n^3\delta(\Delta^2 + (1 + \delta))^2} \\ &\geq \frac{(\Delta^3 - n^2(\delta + \delta^2))^2 (2 + \delta)}{\Delta^2 n^3(\Delta^2 + (1 + \delta))(1 + \delta(\Delta^2 + (1 + \delta)))} \end{aligned}$$

(16)

□

E Appendix: Pytorch Implementation

E.1 Model

```

1 class Transfusion(nn.Module):
2     def __init__(self, num_layers, backbone):
3         super(Transfusion, self).__init__()
4         self.num_layers = num_layers
5
6         # Backbone
7         self.backbone = backbone
8         self.num_ftrs = self.backbone.fc.in_features
9         self.backbone.fc = nn.Sequential([nn.Flatten(), nn.LayerNorm(self.num_ftrs
10    )])
11
12        # TransFusion
13        self.attention_blocks = nn.Sequential(
14            [TransFusionBlock(self.num_ftrs, self.num_ftrs)
15             for _ in range(num_layers)])
16
17        def forward(self, x):
18            x = self.backbone(x)
19            if self.num_layers == 0:
20                fused_embedding = embedding
21            else:
22                fused_embedding = self.attention_blocks(embedding)
23
24            return fused_embedding
25
26
27 class TransFusionBlock(nn.Module):
28     def __init__(self, input_size, output_size, activation):
29         super(TransFusionBlock, self).__init__()
30         self.input_size = input_size
31         self.output_size = output_size
32
33         # Learnable Weights
34         self.query = nn.Linear(input_size, output_size)
35         self.key = nn.Linear(input_size, output_size)
36         self.value = nn.Linear(input_size, output_size)
37
38         self.activation = nn.ReLU()
39
40        def forward(self, x):
41            q = F.normalize(self.query(x))
42            k = F.normalize(self.key(x))
43            v = self.value(x)
44
45            # Calculate Cosine Similarity
46            attn_weights = torch.matmul(q, k.transpose(-2, -1))
47            attn_weights = self.activation(attn_weights)
48
49            # Normalize Weights
50            attn_weights = attn_weights - torch.diag(torch.diagonal(attn_weights))
51            attn_weights = (attn_weights + 1e-10)
52                / torch.sum(attn_weights+1e-10, dim=1, keepdim=True)
53
54            # Apply the attention weights to the value vectors
55            output = torch.matmul(attn_weights, v) + x
56
57            return output
58

```

E.2 Loss Function

```
1
2 class Loss(nn.Module):
3     def __init__(self):
4         super(Loss, self).__init__()
5
6     def forward(self, embeddings, target_affinity):
7         # Normalize the input tensor
8         normalized_zs = F.normalize(embeddings)
9
10        # Compute the affinity matrix
11        affinity = torch.matmul(normalized_zs, normalized_zs.transpose(-2, -1))
12        affinity = affinity**2
13
14        # Normalize Weights
15        affinity = affinity - torch.diag(torch.diagonal(affinity))
16        affinity = (affinity + 1e-10)
17                / torch.sum(affinity+1e-10, dim=1, keepdim=True)
18
19        # Compute the JSD loss
20        loss = F.kl_div((affinity+target_affinity).log(),
21                        target_affinity,
22                        reduction='batchmean')
23        loss += F.kl_div((affinity+target_affinity).log(),
24                        affinity,
25                        reduction='batchmean')
26
27        return loss
28
```